

# A Study of the Effect of Curvature on Fully Developed Turbulent Flow

By FRANK L. WATTENDORF, Ph.D., Research Fellow in Aeronautics,  
California Institute of Technology, Pasadena

(Communicated by H. Bateman, F.R.S.—Received June 28, 1934)

## I INTRODUCTION

1—The solution of many important problems in aeronautics and hydraulics depends largely on the behaviour of turbulent flow along curved surfaces. In flow along plane surfaces the following method has proved to be successful. The laws of turbulent velocity distribution were investigated in straight tubes and channels of constant cross-section and the results applied to the boundary layer with variable thickness.

The present work was undertaken with the idea of isolating the effect of curvature on the turbulent flow as much as possible, by using a curved channel of constant curvature and cross-section. It is hoped that the results of these experiments may be applied later to the general case of curved boundary layers.

## II PREVIOUS WORK ON CURVED FLOW

2—*Hydraulic Experiments*—Most of the previous experimental work on curved flow has been done in connection with special engineering investigations of such problems as pressure loss in pipe bends, and flow in turbines and water channels. Most of the investigations have been made in channels whose depth and breadth were of the same order of magnitude—in other words the mean flow occurring was essentially three-dimensional in character.

In such a flow, the fast-moving particles in the centre section tend to travel outward, are diverted along the walls toward the upper corners, and from there toward the inner wall, thus giving rise to a circulatory motion of two longitudinal vortices. The nature of such flow has been discussed to some extent by Lell,<sup>†</sup> Isaachsen,<sup>‡</sup> Hinderks§, and Nippert.||

<sup>†</sup> "Beitrag zur Kenntnis der Sekundärströmungen in gekrümmten Kanälen," Darmstadt Diss., 1913.

<sup>‡</sup> 'Z. Ver. deuts. Ing.,' vol. 55 (1911).

§ 'Z. Ver. deuts. Ing.,' vol. 71 (1911).

|| 'Forsch. Ing. Wes.,' p. 320 (1929).

If, however, the depth of the channel is large compared with the breadth, the influence of the top and bottom boundaries on the flow is negligibly small and the mean motion at the centre part is approximately two-dimensional. In this case, therefore, the influence of the centrifugal forces on the turbulent flow can be properly studied. The present investigations are restricted to this case.

3—*Betz-Wilcken Experiments*—A series of experiments on two-dimensional flow in curved channels was started by Betz in 1927. Wilcken† made the first investigations on the boundary layer flow in a series of curved channels. In each case the channel depth was large in comparison with the breadth in order to avoid the formation of the above mentioned secondary vortices. Wilcken studied especially the development of boundary layers along curved surfaces and found that the thickness of the boundary layer increases much more rapidly on the concave (outer) surface, than on the convex (inner) surface. He explains this by the supposition that the centrifugal forces at the outer wall promote, and near to the inner wall diminish, the turbulent interchange between fluid layers. The rapid increase of the boundary layer thickness is due, according to this explanation, to the increased interchange. In Wilcken's case, dealing with two boundary layers separated by potential flow, it is difficult to draw any conclusion regarding the influence of the curvature on the turbulence, because the fluid paths are not parallel. We can define as the fully developed state of curved flow the state in which the mean velocities are parallel to the walls and depend only upon the co-ordinate normal to the walls.

4—*Maccoll-Wattendorf Experiments*—In 1929, Maccoll and the present writer used a modified form of the Wilcken apparatus to study the further development of the flow after the boundary layers have come together and approach this fully developed state. In order to obtain a fully developed flow, a straight channel 2 metres in length was built before the curved channel so that the boundary layers met before entering the curved portion of the channel. However, these measurements were of an introductory nature and indicated clearly the need for further systematic work. It was for this reason that measurements were made in an improved type of curved channel at the California Institute of Technology, as reported in this paper.

† 'Ingen. Arch.,' vol. 1, p. 4 (1930).

## III PRESENT WORK

5—*Channels and Motor*—Investigations were made in two different channels, designated I and II, shown schematically in fig. 1.† The channels had a breadth of 5 cm and a depth of 90 cm, so that the ratio of depth to breadth was 18 : 1. The ratio was chosen large to avoid as far as possible any disturbing influence of the top or bottom on the flow, in other words to avoid the formation of the longitudinal vortices

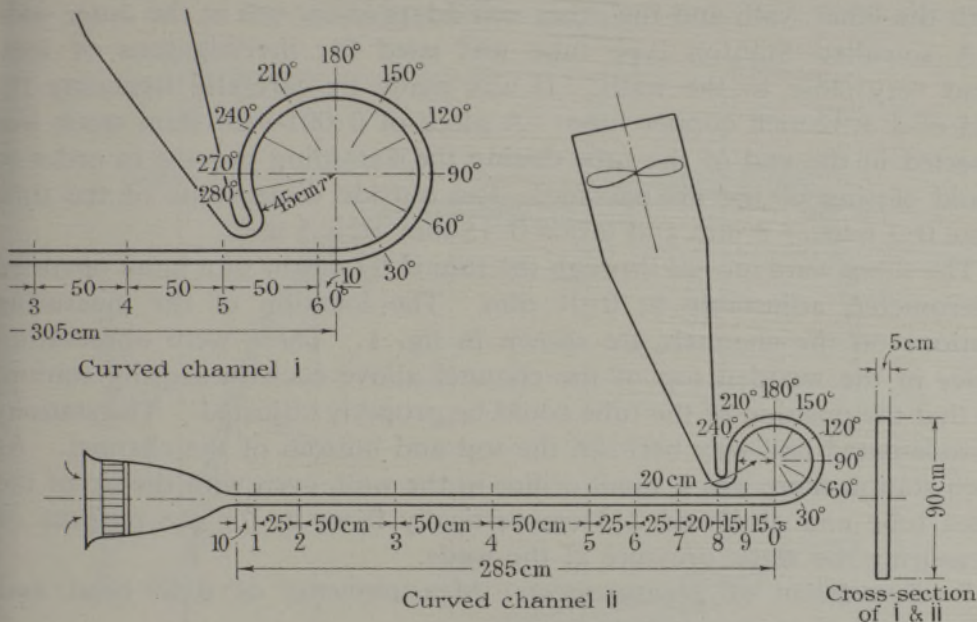


FIG. 1

mentioned in section 2. The channels consisted of the following main parts:—

(a) A bell-shaped intake with a honeycomb built into the large portion of the funnel to straighten out eddies entering from outside.

(b) A straight section 305 cm long (61 times the channel breadth) for the purpose of building up the flow into a fully developed state.

(c) The curved section, with the walls bent in concentric circular arcs, with the radius of the inner wall = 45 cm for channel I, and 20 cm for channel II, and the radius of the outer wall = 50 cm for channel I, and 25 cm for channel II. The curvature extended through about 300° of arc, in order to obtain so far as possible a fully developed curved flow.

† Mr. G. S. Lufkin was largely responsible for the construction of channel I, as well as for preliminary measurements.

This was an improvement over the Göttingen channel of Maccoll and the author which extended only through  $180^\circ$ .

(d) An exit cone which formed the transition between the rectangular channel section and the propeller section 55 cm in diameter.

6—*Pitot Tubes*—The two tubes for measuring total head consisted of copper tubes bent at right angles, each with a short length of hypodermic needle, 0.76 mm in diameter, carefully soldered into its tip. One of the tubes was bent slightly so that the tip would come into good flat contact with the inner wall, and the other was adapted for use at the outer wall.

A so-called Stanton type tube was used for investigations of total head very close to the walls. It was made by carefully flattening the end of a 3/32-inch copper tube. A piece of 0.001-inch shim stock was inserted in the end of the tube during the flattening process in order to avoid closing of the air passage. The outside dimensions of the tube were 0.3 mm  $\times$  3 mm and inside 0.15 mm  $\times$  2.5 mm.

The tubes were moved through the tunnel by means of a hand operated micrometer, adjustable to 0.01 mm. The location of the measuring stations on the channels are shown in fig. 1. There were observation holes in the wooden top of the channel above each measuring station, so that the position of the tube could be properly adjusted. The stations were situated half-way between the top and bottom of the channel. At each station there was a small orifice in the wall, even with the tip of the pitot tube and displaced 2.5 cm vertically from it, for the purpose of measuring the static pressure at the walls.

7—*Description of Measurements*—Measurements of total head and calculation of static pressure.

Measured points of total head readings at the  $180^\circ$  and  $210^\circ$  sections of channel II are shown in fig. 2. It is seen that the curves for the two consecutive measurement stations are quite similar, but displaced by a constant amount equal to the drop in pressure along the channel between the two stations. In straight flow, total head is a maximum at the centre of the channel, but for flow in the present curved channels, the maximum total head is displaced toward the outer wall, and it is fairly flat over a large portion of the channel.

Preliminary work with static pressure tubes indicated that static tubes tend to read too low in turbulent flow. It appears that if a static tube is placed in an air stream of fluctuating direction, the mean value of the pressure reading will be lower than the maximum, the magnitude depending on the percentage of angular fluctuation of the flow. An additional error may also exist in the present case owing to the curvature of the streamlines around the tube. At the wall orifices, however, the fluctuation

normal to the wall must vanish, and the streamlines will be parallel to the wall, so that the readings given by the static orifices are reasonably accurate. For this reason, it was decided to calculate the distribution of static pressure from the readings at the wall orifices, according to the following method :

Let  $u$  and  $v$ , fig. 3, be the tangential and normal components of velocity in a curved flow at radius  $r$  from the centre of curvature. Then

$$dp/dr = \frac{\rho u^2}{r} - \rho u \frac{dv}{rd\theta},$$

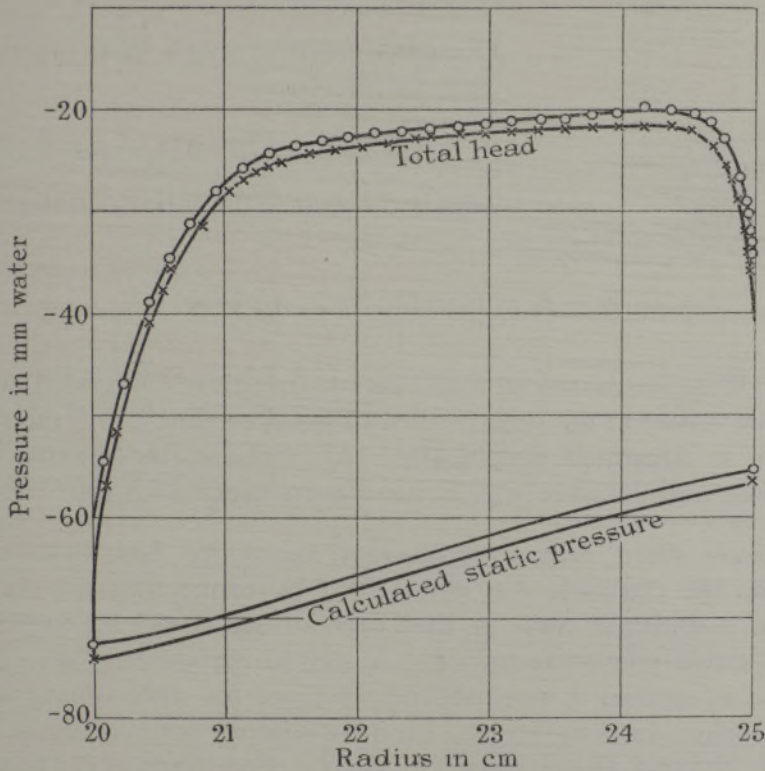


FIG. 2—Total head and static pressure curves for curved channel II, fully developed sections,  $\circ$ ,  $180^\circ$  section ;  $\times$ ,  $210^\circ$  section

if we can neglect the effect of the apparent stresses of the type  $\partial\tau/r\partial\theta$ . The first term represents the centrifugal force, and the second term the pressure due to the normal component of velocity. The second term vanishes for fully developed flow, and even in the transition region is small compared with  $u^2/r$ .

The calculation for the fully-developed region where the second term may be neglected is as follows :

We have

$$dp/dr = \rho u^2/r. \quad (1)$$

Now we assume that the measured value of the total head is accurate enough for our purpose

$$H = p + \frac{1}{2}\rho u^2. \quad (2)$$

It follows from (2)

$$\rho u^2 = 2(H - p)$$

and substituting in (1) gives

$$dp/dr = (2/r)(H - p).$$

Using the pressure at one wall, say the inner wall, as reference,

$$d(p - p_i)/dr = (2/r)[(H - p_i) - (p - p_i)].$$

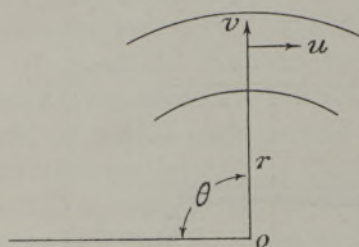


FIG. 3

This is a linear differential equation of the

first order whose solution is

$$p - p_i = (1/r^2) \int_{r_i}^r (H - p_i) 2r dr. \quad (3)$$

$H$  is taken from the measured total head distribution,  $p$  has been measured at the static orifice in the inner wall with good accuracy, and the function  $(H - p_i)r$  is integrated graphically. As a check, the measured value of the outer wall pressure was in good accordance with our calculation.

8—*Pressure Drop Measurements and Resistance Law*—The pressure drop along the channels was determined by connecting the static wall orifices to a multiple cock so that each orifice could be connected in turn to a single micromanometer. A second manometer, connected to the orifice at section 9 was used as reference for maintaining constant velocity during measurements. Pressure distribution curves at several speeds for channel II are shown in fig. 4. For channel I, the pressure drop was measured only in the curved portion of the channel, while for channel II, the straight section was measured as well. It is interesting to note for the case of channel II that the pressures at the outer and inner walls begin to diverge about 20 cm in advance of the beginning of the curvature. From this divergence point to the  $30^\circ$  section the pressure rises at the outer wall and decreases more rapidly at the inner wall until the curves proceed as parallel lines. It should be noticed that for the straight section the pressures are plotted against length and from the beginning of the curvature against angle. The reason for this is that for

resistance law calculations,  $dp/dx$  is used for the straight section, while evaluations of a curved flow are based on the assumptions of a constant  $dp/d\theta$ . That this assumption is justified in the part of the curved channel after the transition stage is seen from the fact that the curves of pressure against angle can be represented by such parallel straight lines.

The resistance coefficient  $\lambda$  for channel II, where measurements were made in both the straight and curved sections was calculated according to the definitions

$$\frac{dp}{dx} = \frac{\lambda}{b} \cdot \frac{1}{2} \rho \bar{u}^2 \quad (4)$$

for the straight portion of the channel, and

$$\frac{dp}{r_c d\theta} = \frac{\lambda}{b} \cdot \frac{1}{2} \rho \bar{u}^2 \quad (5)$$

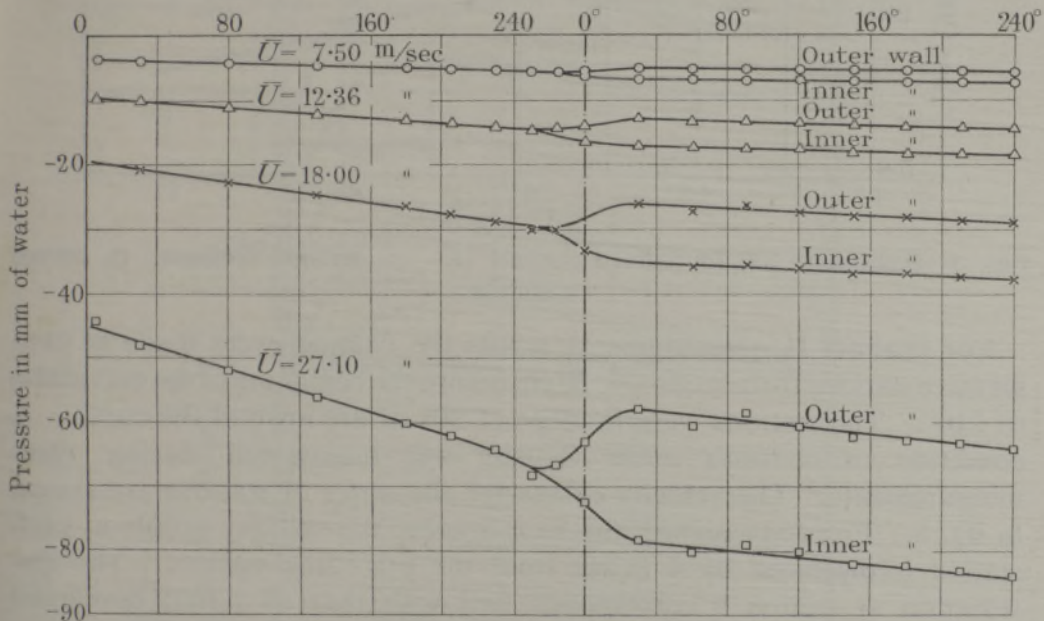


FIG. 4—Pressure distribution along channel walls, curved channel II

for the developed curved portion of the channel. In the above formulæ  $\bar{u}$  = mean velocity,  $b$  = channel breadth, and  $r_c$  = radius of the channel centre line in the curved portion. The pressure drop along the centre line of the curved channel was judged as being the best basis of comparison with straight flow. Fig. 5 shows the result. It is seen that the resistance coefficient for the straight entrance is slightly lower than the Blasius law for straight pipes with circular cross-section, and that the curved portion of the channel has a resistance coefficient only slightly higher. Higher resistance coefficients obtained in pipe bends of about the same

curvature may probably be attributed to the secondary vortices of the three-dimensional mean flow.

9—*Velocity Distribution at Various Stations along Channel*—The velocity distribution was measured at a series of stations along both channels for one Reynolds' number. The velocity was calculated from the curves of total head and static pressure according to the equation

$$H = p + \frac{1}{2}\rho u^2.$$

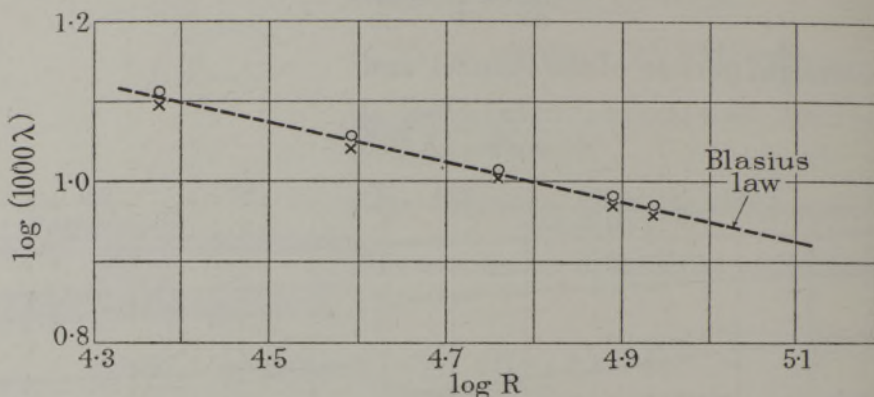


FIG. 5—Resistance law for curved channel II. ×, straight sections; ○, curved section

For channel II, measurements across the channel were made at consecutive stations from section 9, 20 cm before the beginning of the curvature, to 210°. The stations were in steps of 30° of arc around the curve. A condition of constant mean velocity was maintained during these measurements. The velocity curves for the series of stations are shown in fig. 6. For convenience, the base line for the velocity profile at each station is displaced by 4 m/sec from the preceding station. The distribution at section 9 corresponds well with that of a fully developed turbulent flow in a straight channel. The distribution of the 0° section shows the beginning of transition from straight to curved flow. The 30° section shows a strongly distorted profile, with the peak of maximum velocity shifted toward the inner wall. This is in good agreement with the pressure distribution along the wall shown in fig. 4, where we have seen that through this transition region the pressure rises at the outer wall and stops at the inner wall. In a potential curved flow, we would expect a higher velocity at the inner wall in accordance with requirements of constant moment of momentum, *i.e.*, the distribution would have the form

$$ur = \text{constant.}$$

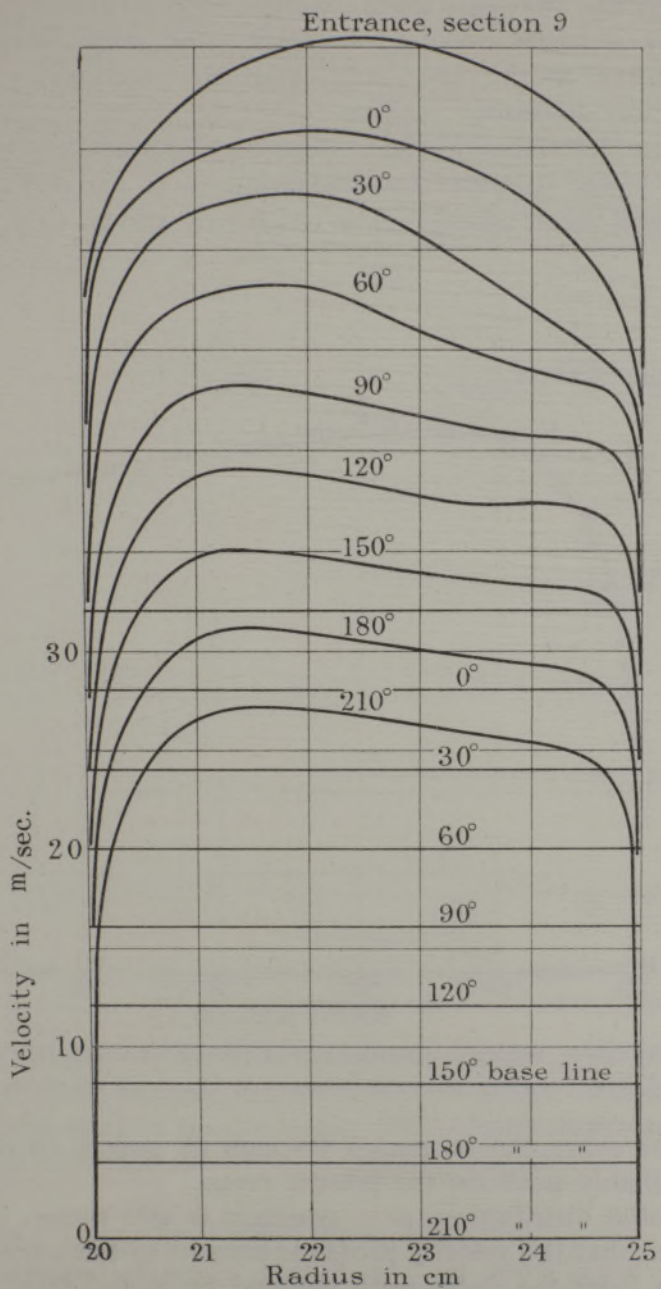


FIG. 6—Velocity distribution in curved channel II

At the  $30^\circ$  section, however, the velocity throughout the inner portion of the channel has increased more than the above formula would require, but after this, it settles down to a steady slope somewhat less than the formula requires, at the  $150^\circ$ ,  $180^\circ$  and  $210^\circ$  sections, which will be termed the fully developed region.

In order to determine if there were any appreciable scale effect in the working range of velocities, distributions at the  $210^\circ$  section were taken at several mean speeds. The results are shown in fig. 7, and it is

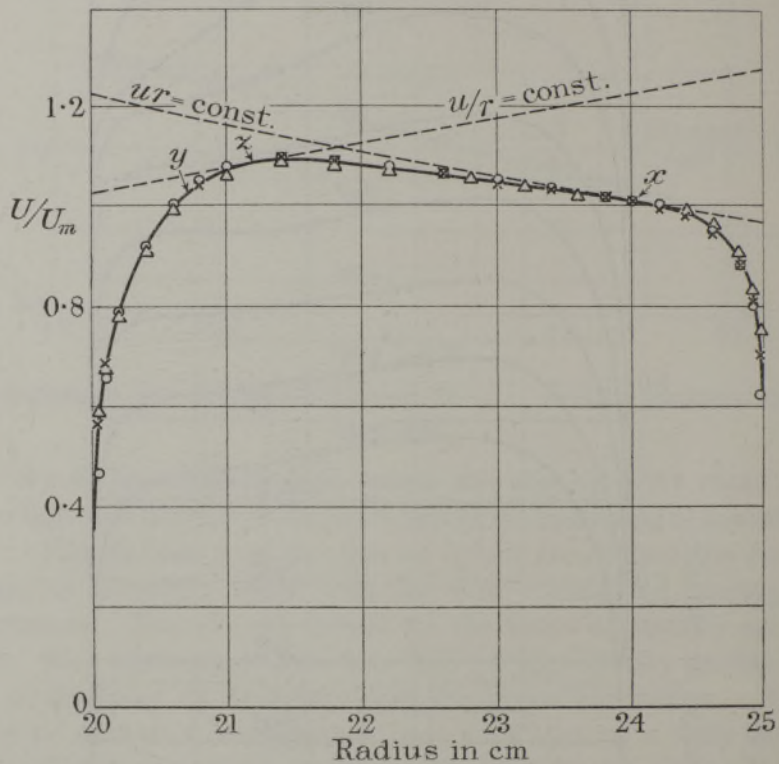


FIG. 7.—Dimensionless velocity distribution in curved channel II.  $\circ$ ,  $U_m = 8.44$  m/sec;  $\times$ ,  $U_m = 17.65$  m/sec;  $\Delta$ ,  $U_m = 25.00$  m/sec

seen that one curve can be passed through all points, so that the scale effect is negligibly small for the present range.

The potential distribution,  $ur = \text{constant}$  is also shown in the figure, and it is seen that the velocity profile is tangent to this curve at a region about 1 cm from the outer wall, denoted by  $x$  and falls only slightly away from it throughout a large central portion of the channel.

The profile at the  $0^\circ$  section of channel I was slightly distorted from the characteristic fully developed profile for straight flow and the transition

to fully developed curved flow was quite similar to that of channel II, except that the slope throughout the central portion was less.

The scale effect for the present velocity range at the  $210^\circ$  section of channel I is seen to be small, see fig. 8. This figure also shows the relation of the distribution to the potential distribution,  $ur = \text{constant}$ .

It is seen that the fully developed profiles for both channels seem to be distorted in the direction of the potential distribution, therefore it seemed of interest to plot the ratio  $ur/(ur)_{\text{max}}$  for both channels, and compare with  $u/u_{\text{max}}$  for straight flow, which should be the limiting case as  $r$

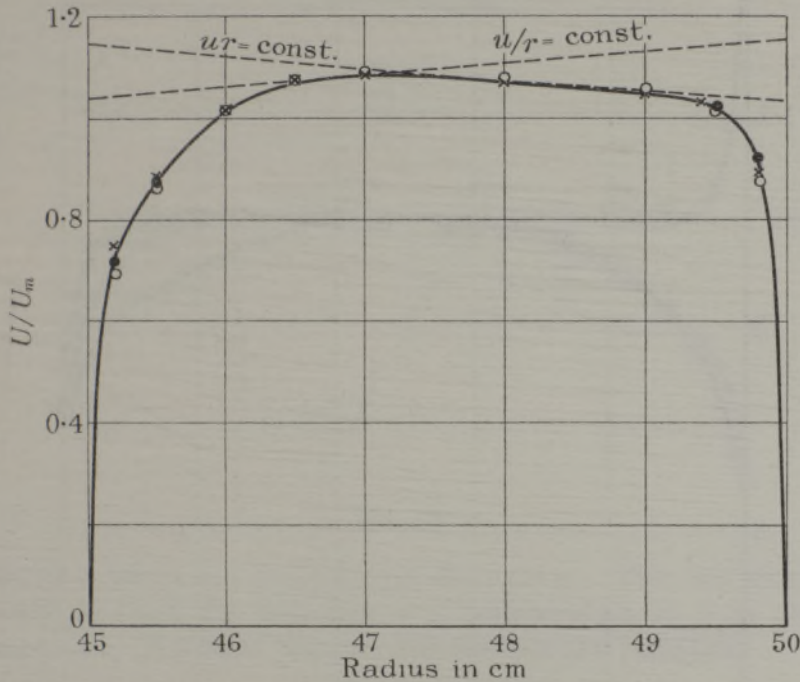


FIG. 8—Dimensionless velocity distribution in curved channel I. ●,  $U_m = 31.0$  m/sec; ×,  $U_m = 25.0$  m/sec; ○,  $U_m = 10.0$  m/sec

approaches infinity. Fig. 9† shows the comparison, and it is remarkable that the difference between the two channels is very small, although the deviation from straight flow is large. This clearly indicates the need for experimental data for channels of weaker curvature.

#### IV THEORETICAL DISCUSSION

10—*Calculation of the  $\tau$  Distribution for the Curved Channel*—The distribution of the shearing stress  $\tau$  for a fully developed curved flow may

† The curve labelled “concentric cylinders” in fig. 9 will be discussed in a later section.

be calculated from a consideration of the moments of momentum about the centre of curvature of the channel.

Consider the forces acting on a small element of fluid in a curved channel. Fig. 10 represents an element at radius  $r$ . The flow is assumed fully developed, that is, there is no change of momentum in the tangential

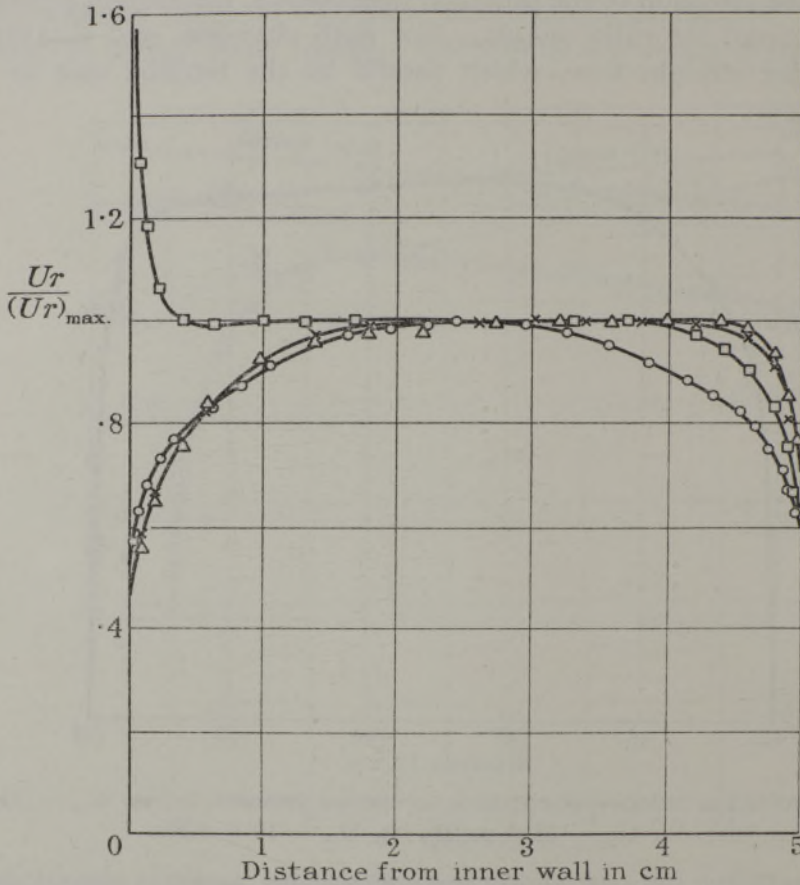


FIG. 9— $U_r/U_r(\max)$  curves for concentric cylinders and curved channel I and II.  
 ○, straight flow; ×, channel I,  $210^\circ$  section; Δ, channel II,  $210^\circ$  section;  
 □, concentric cylinders

direction and the mean value of the normal component is everywhere = 0. The only forces acting are pressure and shearing stress. If we take  $\tau$  as the shearing stress, then the shearing force on the area formed by the arc  $r d\theta$  and unit depth is  $\tau r d\theta$  and the moment of this force about the centre is

$$\tau r^2 d\theta.$$

If  $p$  = pressure, the moment of the pressure about the origin is  $pdr \cdot r$ . Equating moments of force we have

$$\tau r^2 d\theta + \frac{\partial (\tau r^2)}{\partial r} dr d\theta - \tau r^2 d\theta = \left( pdr + \frac{\partial p}{\partial \theta} d\theta - pdr \right) r$$

or

$$\frac{\partial (\tau r^2)}{\partial r} = \frac{\partial p}{\partial \theta} \cdot r.$$

Integrating

$$\int \frac{\partial (\tau r^2)}{\partial r} dr = \int \frac{\partial p}{\partial \theta} r dr$$

or

$$\tau r^2 = \frac{\partial p}{\partial \theta} \frac{r^2}{2} + C,$$

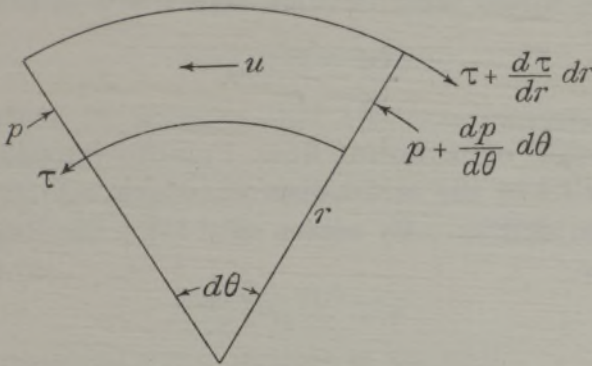


FIG. 10

where  $\partial p / \partial \theta$  is taken as constant over the radius. This last assumption can be derived from the fact that  $u$  is independent of  $\theta$  in the fully developed flow. We have only to differentiate the equation

$$\frac{\partial p}{\partial r} = \rho \frac{u^2}{r}$$

with respect to  $\theta$ , which gives

$$\frac{\partial^2 p}{\partial r \partial \theta} = 0 \quad \text{or} \quad \frac{\partial p}{\partial \theta} \quad \text{is independent of } r.$$

The constant of integration may be determined if we know the value of  $\tau$  at one point. If we take the point in the channel where  $\tau = 0$  as reference, and call the radius at this point  $r_m$ , we have

$$c = - \frac{\partial p}{\partial \theta} \frac{r_m^2}{2}$$

and finally,

$$\tau = \frac{1}{2} \frac{\partial p}{\partial \theta} \left[ 1 - \left( \frac{r_m}{r} \right)^2 \right]. \quad (6)$$

The choice of  $r_m$  has been the subject of some discussion arising from various physical interpretations of  $\tau$ . For laminar flow in a curved path, we have

$$\tau = \mu \left( \frac{\partial u}{\partial r} - \frac{u}{r} \right), \quad (7)$$

where  $\mu$  is the coefficient of viscosity of the fluid. It is customary to use an analogous expression for  $\tau$  in a turbulent flow, namely,

$$\tau = \rho \varepsilon \left( \frac{\partial u}{\partial r} - \frac{u}{r} \right), \quad (8)$$

where  $\varepsilon$  represents the "apparent" coefficient of kinematic viscosity, or "exchange coefficient" of the turbulent mixing process. From this point of view it would seem obvious that  $\tau = 0$  when

$$\frac{\partial u}{\partial r} - \frac{u}{r} = 0.$$

In his discussion of turbulent flow, Prandtl† introduces the so-called "mixing length"  $l$  or the mean distance which a fluid element travels before losing its identity. By means of " $l$ ,"  $\tau$  may be expressed for a straight flow as

$$\tau = \pm \rho l^2 \left( \frac{\partial u}{\partial y} \right)^2. \quad (9)$$

By an analysis (discussed more fully in section 13) in which he assumes that a displaced fluid element in curved flow maintains its moment of momentum, Prandtl gives as the expression for  $\tau$  in a curved flow

$$\tau = \pm \rho l^2 \left( \frac{\partial u}{\partial r} + \frac{u}{r} \right)^2, \quad (10)$$

whereby it is seen that  $\tau = 0$  for  $\frac{\partial u}{\partial r} + \frac{u}{r} = 0$ .

Since most theoretical discussions involve a knowledge of the  $\tau$  distribution, the importance of determining  $\tau$  experimentally is evident. It was for this reason that an approximate method of determining  $\tau_0$  at the walls, by means of the Stanton tube, was developed for channel II.

11—*Measurement of Shearing Stress at the Walls*—The Stanton tube used for the shearing stress measurements had a mouth opening of dimensions about 0.15 mm  $\times$  2.5 mm. For orifices of such small dimensions, Stanton found that the total head reading of the tube does

† 'Verh. int. Kong. Tech. Mech. Zürich,' 1926.

not correspond with the total head at the geometrical centre of the tube but with the pressure at an "effective" centre, at a distance  $\delta^*$  from the wall of the channel, when the tube is in contact with the wall. Stanton† determined the effective centre by calibrating his tubes in a channel where the flow was laminar in character. For the present experiments, however, an approximate method was used, as follows:

The shearing stress  $\tau_0$  at the wall of the straight entrance section is determined by the pressure drop,

$$\tau_0 = b/2 (dp/dx),$$

where  $b$  is the breadth of the channel. In the region quite close to the wall we have a so-called "laminar sub-layer," where the shearing stress is given essentially by the formula

$$\tau_0 = \mu (\partial u / \partial y)_0,$$

$\mu$  is the coefficient of viscosity and  $(\partial u / \partial y)_0$  represents the velocity gradient at the wall.

If we define the distance from the wall to the effective centre as  $\delta^*$ , and the reading of the total head of the tube as  $H^*$ , then the effective velocity is given as

$$\frac{1}{2} \rho u^{*2} = H^* - p,$$

where  $p$  = the measured static pressure at the wall.

We have then for  $\tau_0$  approximately

$$\tau_0 = \mu (U^* / \delta^*)$$

from which  $\delta^*$  may be calculated, since  $\tau_0$  is known for the straight channel. Now we assume that  $\delta^*$  is the same function of  $U^*$  and the breadth of the orifice of the Stanton tube in the curved channel as has just been found in the straight channel, when in both cases the Stanton tube is in contact with the wall.  $\tau_0$  for the curved channel is determined from the measured  $U^*$  and the corresponding value of  $\delta^*$  taken from the curve of  $\delta^*$  vs.  $U^*$ .

In each case  $\delta^*$  is determined at several speeds so that the value of  $\tau_0$  can be plotted against Reynolds' number while the other physical parameters involved, such as the breadth of the orifice, and  $\mu$  remain unchanged. The Reynolds' number is based on the mean velocity in the channel, and the channel breadth  $b$ .

Curves of the distribution of  $\tau$  in the fully developed curved region of channel II, at  $R = 25400$ , on the basis of several different assumptions

† Stanton, Marshall and Bryant, 'Proc. Roy. Soc.,' A, vol. 97, p. 413 (1920).

as to the point where  $\tau = 0$  are shown in fig. 11. Curve *a* corresponds to the assumption that  $\tau = 0$  for  $\frac{\partial u}{\partial r} + \frac{u}{r} = 0$ , whereby  $r_m = 24.0$ , curve *c* corresponds to  $\tau = 0$  for  $\frac{\partial u}{\partial r} - \frac{u}{r} = 0$ , whereby  $r_m = 21.2$  cm.

The actual value of  $\tau_0$  at the walls as determined by the Stanton tube measurements at this Reynolds' number are indicated by the two small

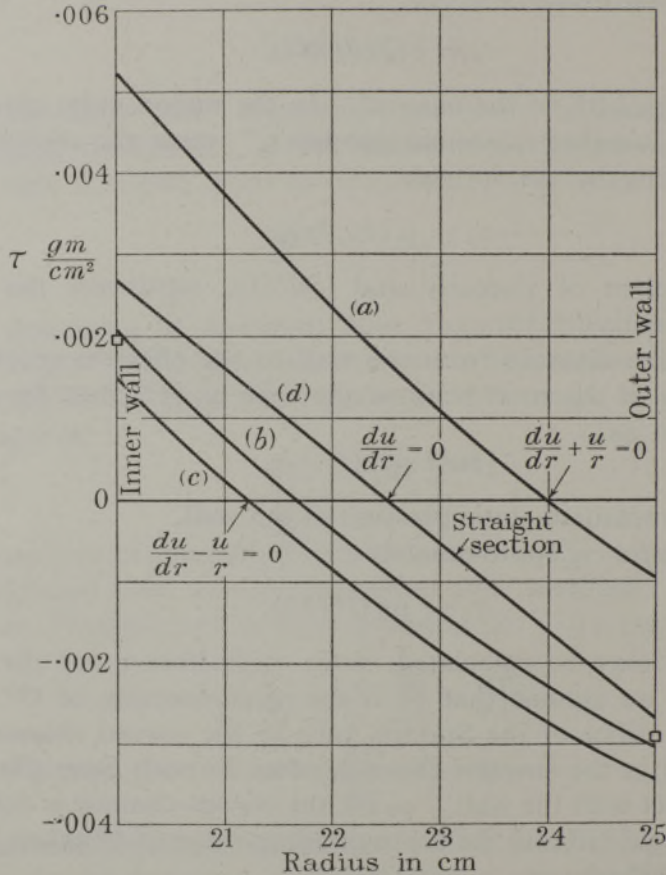


FIG. 11—Distribution of  $\tau$  for curved channel II

squares. Curve *b* is the calculated curve which most nearly satisfies both wall values. This curve passes through zero at the point  $r_m = 21.7$ , which lies between the curves *c* and *a*, although close to *c*.

Physically this may mean that since both expressions for  $\tau$  represent approximations to the true conditions, they may both be partly right, and the actual flow may be a combination of several processes, so that the corresponding curve lies between the two theoretical curves. The

ucceeding evaluation of results for channel II was made on the basis of the curve  $b$  corresponding to the measured wall points. ( $r_m = 21.7$ )

12—*Measurements with Concentric Cylinders*—It was thought of interest to compare the flow in the curved channel with the Couette type of curved flow, namely flow between concentric cylinders. For this purpose a rotating cylinder apparatus, shown in fig. 12, was built, in which the inner cylinder rotated while the outer was stationary. The radius of the inner cylinder was 20 cm and that of the outer 25.4, so that the curvature was nearly the same as that for channel II.

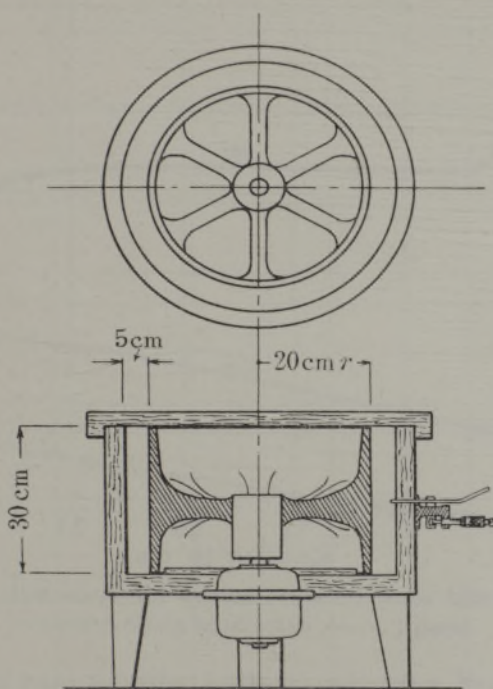


FIG. 12

For comparison with the curved channel, consecutive measurements were made with the Stanton tube, first at the outer wall of the curved channel, and then at the wall of the stationary outer cylinder. In order to obtain equal wall friction for the two cases, the speed of the inner rotating cylinder was adjusted until the reading of the Stanton tube was the same as for the curved channel. This condition was found to occur when the product  $ur$  in the centre region between the cylinders, where approximately  $ur = \text{constant}$ , was the same as the maximum value of  $ur$  for the curved channel. The distribution of  $ur/(ur)_{\text{max}}$  for the cylinders,

compared with the curves for the curved channels, is shown in fig. 9. For the cylinders,  $(ur)_{\max}$  represents the maximum value of  $(ur)$  excluding the region near the inner cylinder.

Fig. 13 shows the measured total head and calculated static pressure distribution for the cylinders. It is seen that the total head is practically constant throughout a large region, corresponding to the condition of a flow with constant circulation. Dimensionless velocity distributions for two speeds are shown in fig. 14.

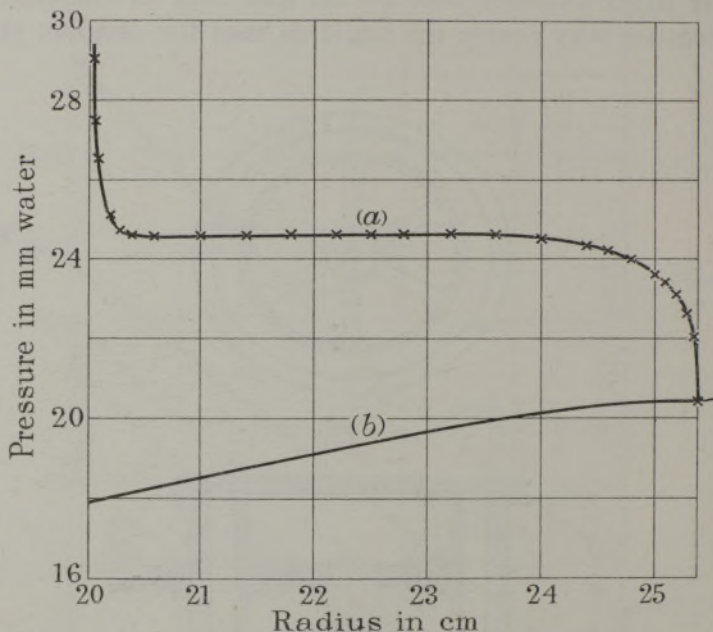


FIG. 13—Total head and static pressure curves for concentric cylinders.  $\times$ , total head ; —, calculated static pressure

The distribution of  $\tau$  for the rotating cylinder may easily be calculated from the value measured by the Stanton tube at the outer wall, using the equation of constant moment of force

$$\tau r = \text{constant.}$$

The value of  $\tau_i$  for the inner wall is then given by

$$\tau_i = \tau_0 r_0 / r_i.$$

As a check on the accuracy of the Stanton tube measurement, the value of  $\tau_i$  for the inner cylinder obtained by the calculation first mentioned was compared with measurements of Wendt, of Göttingen, who

actually measured the torque on the inner rotating cylinder in a similar experiment with water. The values check within 3%.

13—*Discussion of Prandtl's Theory for Curved Flow*—The influence of curvature on turbulent flow has been discussed by Prandtl.† His considerations are an extension of Rayleigh's‡ investigations on the stability of curved flow in an ideal fluid. Rayleigh's theory will be briefly reproduced below.

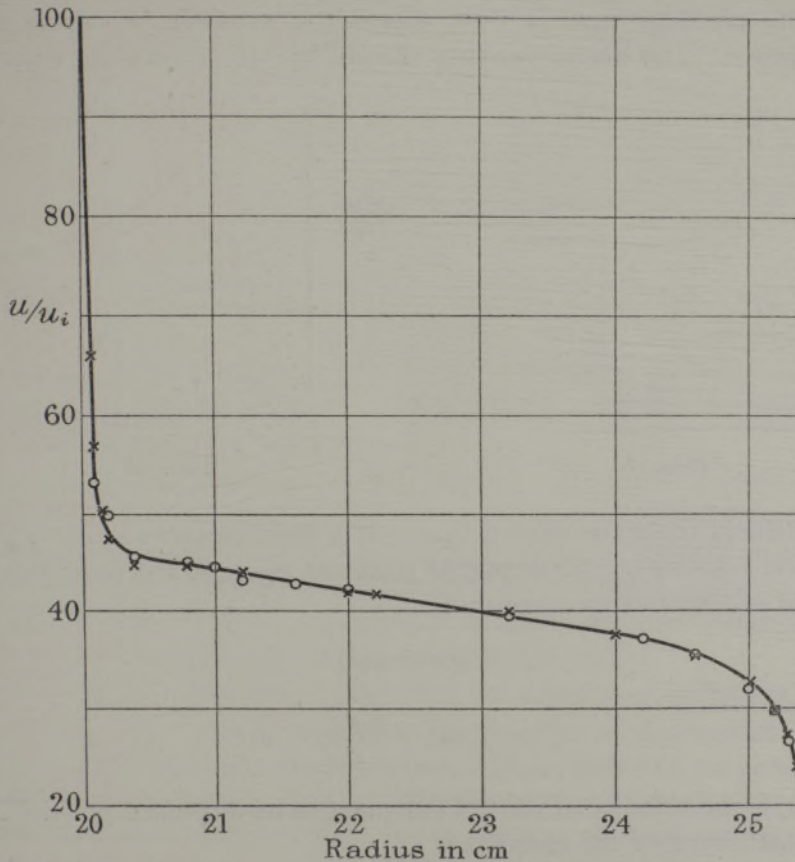


FIG. 14—Velocity distribution between concentric cylinders, inner cylinder rotating ; outer cylinder stationary.  $\circ$ ,  $U_i = 22.8$  m/sec;  $\times$ ,  $U_i = 36.4$  m/sec  
 $U_i$  = tangential velocity at inner cylinder

Consider the undisturbed flow of a fluid in a curved path, fig. 15. If a fluid element moving with tangential velocity  $u$  at a distance  $r$  from the centre of curvature  $o$ , be displaced by a disturbing force acting along the radius, the moment of momentum of the element, taken around the axis

† 'Vorträge aus dem Gebiete des Aerodynamik Aachen Ks.' (1929), p. 1.

‡ "On the Dynamics of a Revolving Fluid," Sci. Pap., vol. 6 (1916).

perpendicular to  $u$  through  $o$ , must remain unchanged, since there is no component of the disturbing force in the tangential direction. In the undisturbed flow, the pressure gradient along  $r$  is in equilibrium with the centrifugal force.

$$\frac{\partial p}{\partial r} = \rho \frac{u^2}{r} \quad (11)$$

neglecting smaller order terms, such as friction.

Let us consider now a flow where the product  $ur$  decreases with increasing  $r$ . The accompanying sketch, fig. 16, shows the distribution

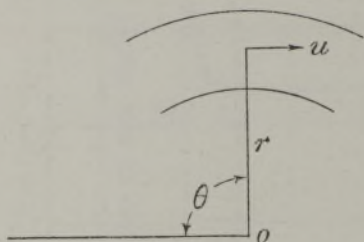


FIG. 15

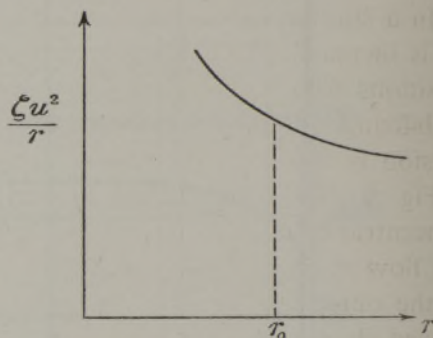


FIG. 16

of centrifugal force for such a case. If a fluid element at  $r = r_0$ , where it has the velocity  $u_0$ , be displaced outward along  $r$ , the requirement for constant moment of momentum is

$$u_e r = u_0 r_0$$

or

$$u_e = \frac{u_0 r_0}{r},$$

where  $u_e$  is the velocity of the fluid element in its displaced position. The centrifugal force of the element is

$$\rho \frac{u_e^2}{r} = \rho \frac{u_0^2 r_0^2}{r^3}. \quad (12)$$

We have chosen, however, a flow with decreasing value of  $ur$  along the radius, so that  $u < \frac{u_0 r_0}{r}$  for  $r > r_0$ , where  $u$  is the local fluid velocity.

Hence for the centrifugal force

$$\rho \frac{u^2}{r} < \rho \frac{u_0^2 r_0^2}{r^3}. \quad (13)$$

Substituting equations (1) and (2) in the above inequality we have

$$\frac{dp}{dr} < \frac{\rho u_e^2}{r}. \quad (14)$$

Hence the centrifugal force of the displaced fluid element is greater than the centripetal pressure gradient, and the motion is unstable, because the tendency is for the displaced particle to move further in the same direction. Conversely, if the displacement is inward, the centrifugal force will be less than the centripetal pressure gradient, and the element will be forced further inward.

In a similar manner we arrive at the conclusion that in a flow where  $ur$  is increasing outward, the elements displaced from their equilibrium positions will be forced back to their positions, and the action will be stabilizing. If we are dealing with a flow where  $ur = \text{constant}$  the conclusion is that the stability is neutral.

Fig. 9 shows the curves  $ur/(ur)_{\max}$  for the curved channels and the concentric cylinders. Applying Rayleigh's criterion, it is concluded that the flow is unstable at both walls of the concentric cylinders as well as at the outer wall of the curved channel, while at the inner wall of the curved channel the flow is stable.

This instability criterion was first stated as far as the author is aware by Rayleigh (*loc. cit.*) in 1916 and was applied and refined by taking the viscosity effect into consideration by G. I. Taylor† in 1923 in his work on the instability of laminar flow between two rotating cylinders. Later this criterion was found independently by Bjercknes and Solberg‡ in the course of their meteorological investigations in 1927.

Prandtl applies Rayleigh's reasoning to developed turbulent flow in the following way: he assumes that the transfer of momentum between circular sheets is due to a displacement of fluid particles perpendicularly to the mean streamlines. For this displacement it is assumed, according to Rayleigh's considerations, that the product  $ur$  remains constant. The path of convection or mixing length will be denoted by  $l$ , and the mean value of velocity by  $u$ . Obviously the moment of the shearing stress  $\tau r$  is equal to the transfer of moment of momentum per unit area. This latter quantity is given by

$$\rho l v \frac{d(ur)}{dr}.$$

Thus we obtain the equation

$$\tau r = \rho l v \frac{d(ur)}{dr}$$

† 'Phil. Trans.,' A, vol. 223, p. 289 (1922).

‡ 'Avh. norske Vidensk Akad.,' vol. 50, No. 7, Oslo (1929).

or

$$\tau = \rho l v \frac{d(ur)}{rdr}. \quad (15)$$

The quantity

$$\frac{d(ur)}{rdr} = \frac{du}{dr} + \frac{u}{r}$$

represents the amount of vorticity at the point considered. This formula is identical with Prandtl's formula for shearing stress in parallel motion except that the slope of the velocity is replaced by  $\frac{du}{dr} + \frac{u}{r}$ . In both cases the vorticity is the same.

Using the expression (15) for the turbulent shearing stress, Prandtl concludes from energy considerations that turbulent motion can be permanently maintained when, assuming  $u > 0$

$$(a) \quad \frac{du}{dr} + \frac{u}{r} < 0$$

or

$$(b) \quad \frac{du}{dr} + \frac{u}{r} > 0 \quad \text{and} \quad \frac{du}{dr} - 2\frac{u}{r} > 0.$$

Prandtl concludes from his energy considerations, that the stabilizing effect depends on the value of the parameter  $\theta = \frac{u/r}{du/dr - u/r}$ . If  $\theta$  is positive  $l$  is decreased (stabilizing effect), if  $\theta$  is negative  $l$  is increased (labilizing effect) in comparison with the value of  $l$  prevailing at a corresponding place in a straight channel.

Unfortunately essential difficulties are encountered in attempting to apply the conclusions of Prandtl's theory over the whole range of the channel.

Firstly, the formula (15) requires that  $\tau$  should become zero at the point at which the maximum of  $ur$  is reached. If the shearing stress is represented by a transfer of the quantity  $ur$  by the mechanism assumed by Prandtl, it must have opposite sign in the ranges of increasing and decreasing values of  $ur$ . Accordingly the shearing stress distribution would correspond to curve (a) in fig. 11.

Secondly, according to the Prandtl criterion, turbulent motion can only exist under the conditions (a) or (b) above. These are satisfied between the inner wall and the point  $y$  and between the outer wall and the point  $x$ , fig. 7. Therefore, the criterion obviously cannot be applied between  $x$  and  $y$ , *i.e.*, in the centre part of the channel. Hence, the conclusion must be drawn that the Prandtl theory is not suitable for describing

the turbulent exchange in curved flow except perhaps in the neighbourhood of the walls.

It is easy to see that Prandtl's parameter  $\theta$  is positive at the inner wall and negative at the outer, so that a stabilizing effect is to be expected at the inner wall and a labilizing effect at the outer one.

We arrive at the same result if Rayleigh's simple criterion is used as an indication for the stabilizing or labilizing effect. The essential difference is that the region of zero stabilizing effect would coincide, according to Prandtl's conception, with the point  $\frac{du}{dr} = +\frac{u}{r}$ , while according to Rayleigh's criterion, it would coincide with the point  $\frac{du}{dr} = -\frac{u}{r}$ . It is not possible to decide between these alternatives, but the experiments indicate that the general conclusions of both are valid in the regions near the walls.

$\tau_0$  has been measured for channel II so that the product  $lv = \varepsilon$ , also called exchange factor, can be calculated. In order to carry out these calculations the slope  $du/dr$  has to be determined. Graphical differentiation of velocity curves appeared to be a rather inexact procedure, therefore the following method, suggested by von Kármán, was used. Fig. 17 represents

$$\frac{u}{\sqrt{\tau_0/\rho}} = g \left[ \log \frac{y\sqrt{\tau_0/\rho}}{\nu} \right]$$

denoting the  $\log y\sqrt{\tau_0/\rho}$  by  $x$

$$\frac{du}{dy} = \sqrt{\tau_0/\rho} \frac{dg}{dx} \cdot \frac{1}{y}.$$

Now  $dg/dx$  can be determined with a fair accuracy (*cf.* fig. 17) and so

$$\varepsilon = \frac{\tau}{\rho \left( \frac{du}{dr} + \frac{u}{r} \right)}$$

can be obtained. In order to compare the exchange factors for the straight and curved channel the dimensionless quantity  $\varepsilon/b\bar{u}$  is used, where  $b$  = channel breadth and  $\bar{u}$  = mean velocity in the channel. In fig. 18 the three curves are compared. It is seen that the exchange factor is less than for the straight flow at the inner wall, and greater at the outer wall, which is in accordance with our expectations of stability at the inner wall and instability at the outer wall.

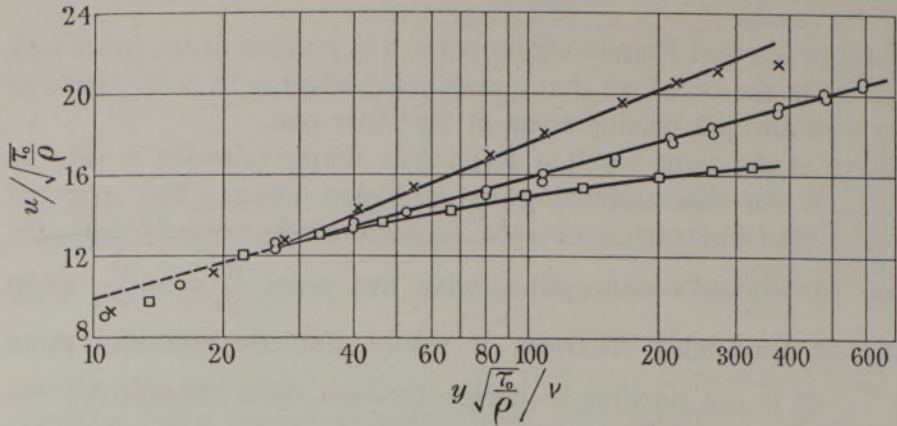


FIG. 17—x, Inner wall, curved channel II; O, straight section; ■, outer wall curved channel II

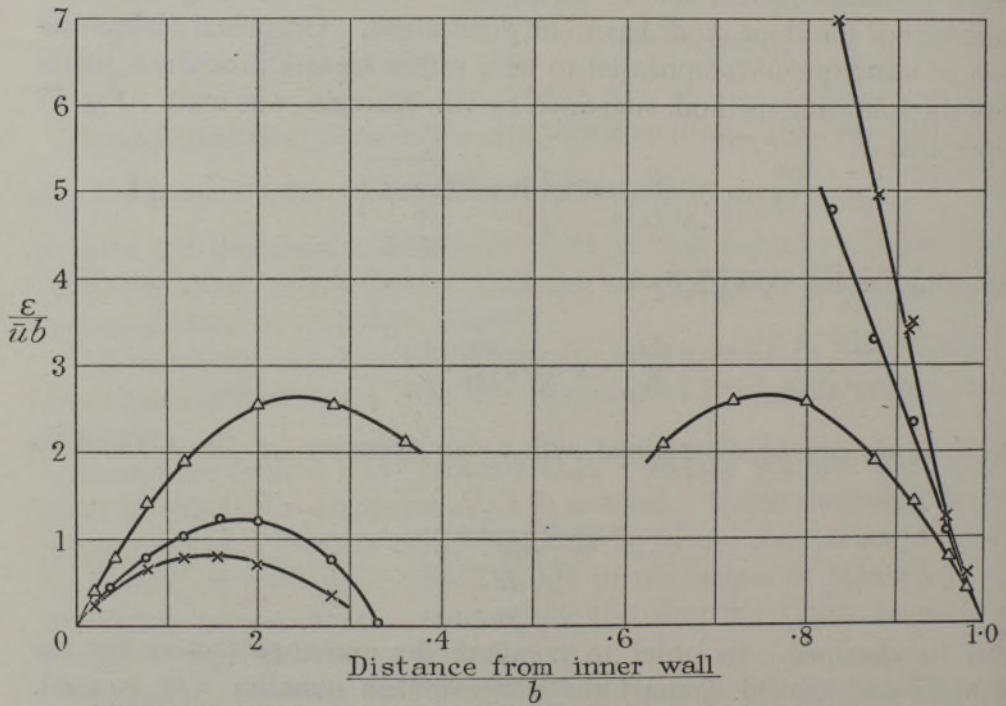


FIG. 18— $\epsilon$  distribution for straight and curved channel;  $\Delta$ , straight flow;

$$\text{O}, \epsilon = \frac{\tau_0/\rho}{\frac{du}{dr} - \frac{u}{r}}; \quad \text{x}, \epsilon = \frac{\tau_0/\rho}{\frac{du}{dr} + \frac{u}{r}}$$

The calculation of the mixing length  $l$  is somewhat uncertain, because the expression for the relation between the normal velocity  $v$  and  $l$  is not definitely known. Prandtl himself has used different expressions in different publications. For the straight channel,  $v$  can be expressed as  $v = l \frac{du}{dy}$ , but it is difficult to see which of the generalizations for curved flow, namely,  $v = l \left( \frac{du}{dr} + \frac{u}{r} \right)$  or  $v = l \left( \frac{du}{dr} - \frac{u}{r} \right)$  is more justified. The mixing length calculated for both assumptions is shown in fig. 19.

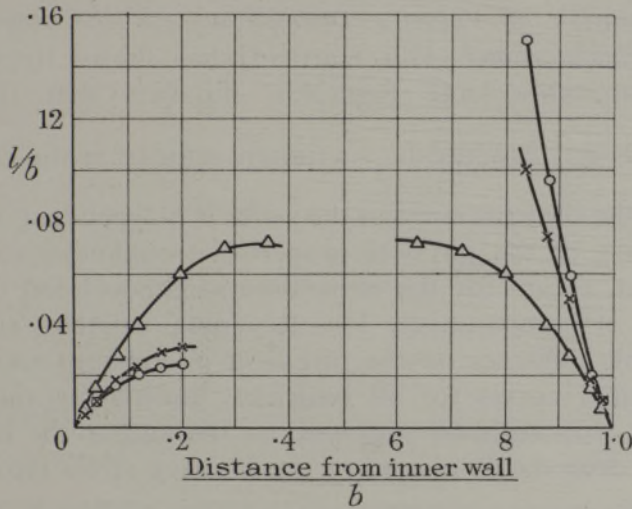


FIG. 19. Δ, straight flow; ○,  $l = \sqrt{\frac{\epsilon}{\frac{du}{dr} + \frac{u}{r}}}$ ; ×,  $l = \sqrt{\frac{\epsilon}{\frac{du}{dr} - \frac{u}{r}}}$

14—*The Exchange Coefficient*—The difficulty of deciding between the expressions  $\frac{du}{dr} + \frac{u}{r}$  and  $\frac{du}{dr} - \frac{u}{r}$  which has appeared in the preceding section is also made apparent by a discussion of the exchange coefficient  $\epsilon$  which was defined in section 10. Whereas, according to Prandtl's reasoning we wrote  $\frac{\tau}{\rho} = \epsilon \left( \frac{du}{dr} + \frac{u}{r} \right)$ , in the generalization of the equation for laminar flow we have to assume  $\tau$  proportional to the rate of shear, i.e.,  $\frac{\tau}{\rho} = \epsilon \left( \frac{du}{dr} - \frac{u}{r} \right)$ . If such an assumption is justified, then the shearing stress would disappear at the point where  $\frac{du}{dr} = + \frac{u}{r}$ . This point can be determined by drawing a tangent from the centre of curvature to the

velocity distribution curve. The corresponding curve is given in fig. 11, curve *c*.

The point  $\tau = 0$  obtained in this way is nearer to that obtained from the actual measurements than the point where the vorticity = 0, but the difference is also too considerable to be explained by inexact measurements. It seems to be probable that the shearing stress in curved flow is not the determining factor for the velocity distribution. Other possible explanations for the measured velocity distributions are given in a later section.

15—*Representation of Velocity Distribution for the Region Outside of the Wall Neighbourhood*—von Kármán† has shown for the straight channel at reasonably large Reynolds' numbers that the function

$\frac{u_{\max} - u}{\sqrt{\tau_0/\rho}}$ , where  $u_{\max}$  denotes the maximum velocity in the centre of the channel and  $\tau_0$  the shearing stress at the walls, is independent of Reynolds' number and also of the physical properties (roughness) of the walls. This means that, except for the immediate neighbourhood of the walls and the range of comparatively low Reynolds' number, the viscosity has no noticeable influence on the turbulent interchange and we obtain a family of similar curves for all velocities, dimensions and grades of roughness. Dr. von Kármán suggested to the author the introduction of the pressure drop  $dp/dx$  instead of the shearing stress into this representation, so that the universal function becomes  $\frac{u_{\max} - u}{\sqrt{1/\rho \cdot \frac{dp}{dx} \cdot b}}$ . Here

$b$  represents one-half the width of the channel considered. The author tried to extend this method of representation to the curved channel. Using von Kármán's representation for the straight flow  $u_{\max} - u$  represents the difference between the velocity corresponding to a uniform or potential flow and the actual velocity. In curved flow it seems to be logical to take the difference between the velocity corresponding to the potential flow,  $ur = \text{constant}$ , and the actual velocity. Accordingly, the curve  $ur = \text{constant}$  has been drawn tangential to the measured velocity distribution curve. The velocity corresponding to the first curve is denoted with  $u_p$  and the difference  $u_p - u$  is used in the representation. By this procedure the channel is divided into two unequal parts, and it is logical to use instead of the half breadth  $b$ , the distances from the point corresponding to  $(ur)_{\max}$  to the two walls, denoted by  $b_e$ .

† 'Nach. Ges. Wiss. Gött.', p. 58 (1930).

The function  $\frac{u_p - u}{\sqrt{\frac{1}{\rho} \cdot \frac{dp}{r_p d\theta} \cdot b_e}}$  is plotted in fig. 20 as function of  $y/b_e$ ,

where  $y$  denotes the distance from the reference point ( $ur = (ur)_{\text{max}}$ ) to the walls, and  $r_p$  denotes the radius of the reference point.

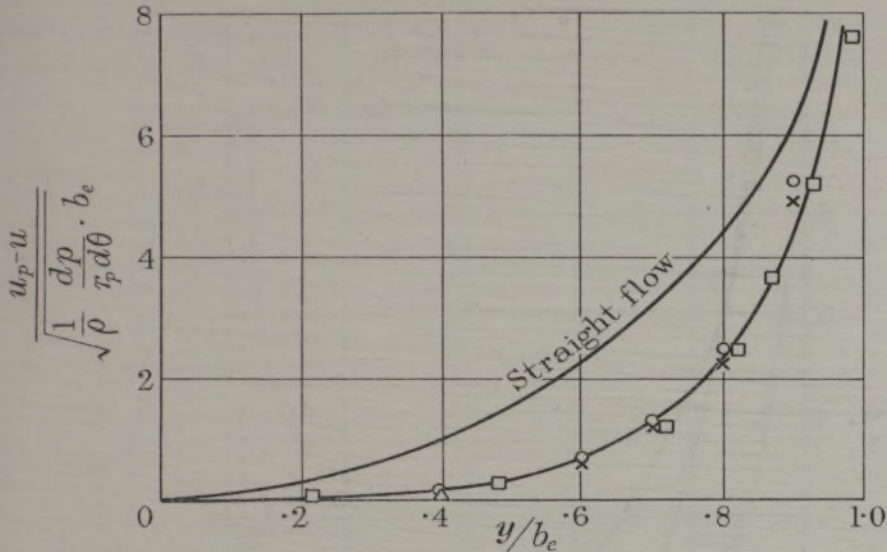


FIG. 20—Dimensionless velocity distributions in curved channels I and II.  $\blacksquare$ , Channel I inner;  $\Delta$ , channel II inner;  $\circ$ , channel I outer;  $\times$ , channel II outer

It is a remarkable coincidence that a single curve can be drawn through the points obtained from the velocity distribution for both walls of the two channels of different curvature. Hence all these four velocity distributions appear as similar. However, it should be noted that the velocity distribution corresponding to the straight flow shows a distinctly different character.

The author feels that before definite conclusions can be drawn from this similarity relation for the velocity distribution, further experiments, especially with weaker curvature, are necessary.

It is evident that the above representation cannot be applied to the rotating cylinders, since in this case  $\frac{dp}{d\theta} = 0$ . However, another procedure was followed, whereby similarity was obtained between the cases of equal curvature (channel II and cylinder), namely, the outer wall of the channel and the outer cylinder, and the inner wall of the channel and the inner cylinder. For the inner rotating cylinder, the velocity relative to the cylinder must, of course, be used for the comparison. The representation

differs from that mentioned in the last paragraph in that  $u_p - u$  is divided by  $\sqrt{\tau_0/\rho}$ , where  $\tau_0$  denotes the measured shearing stress at the walls. The dimension  $b_e$  is the same as before for the channel, but for the cylinder it denotes the breadth in which the product  $ur$  changes from its value at the wall to the constant value which it maintains through the greater part of the

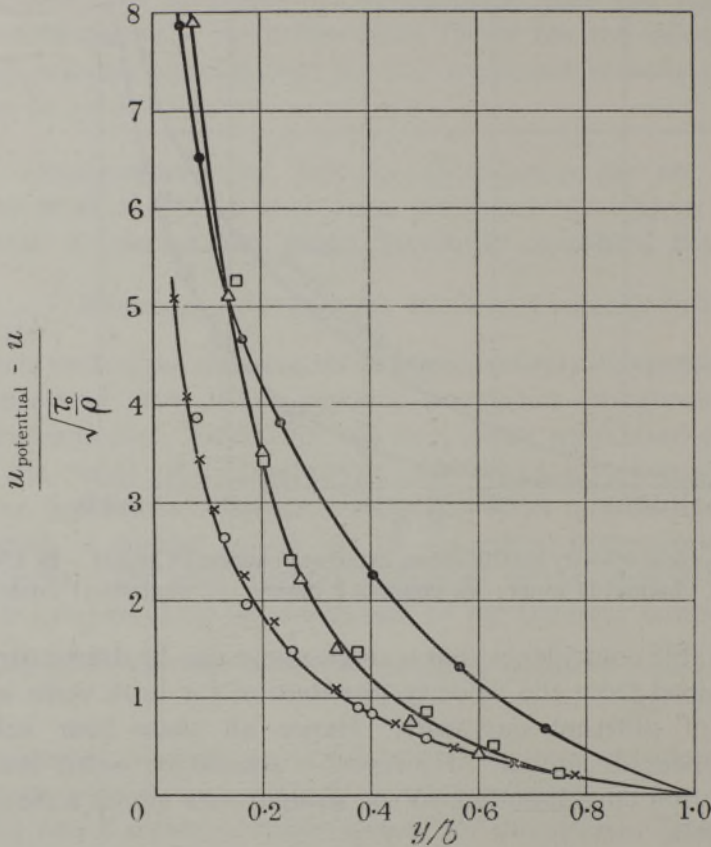


FIG. 21.—Curves of  $\frac{u_{\text{potential}} - u}{\sqrt{\tau_0/\rho}}$  where  $\tau_0$  = measured wall friction

○, curved channel II outer wall; ×, outer cylinder; △, curved channel II inner wall; ■, inner rotating cylinder; ●, straight channel

region between the cylinders. The breadth  $b_e$  is only about 4 mm at the inner cylinder, and about 18 mm at the outer cylinder. The dimensionless velocity curves representing  $\frac{u_p - u}{\sqrt{\tau_0/\rho}}$  as a function of  $y/b_e$  where  $y$  denotes the distance from the reference point as before, is shown in fig. 21.

16—*Discussion of Taylor's Considerations of Vorticity Transport*—In the considerations of the last section, the introduction of the pressure drop seems to be purely arbitrary. However, some justification can be found by following the ideas of G. I. Taylor† concerning the mechanism of turbulent interchange. Taylor considers the transfer of vorticity between adjacent fluid layers in a turbulent flow, and shows that for a two-dimensional parallel mean flow, the transfer of vorticity is proportional to the pressure drop. In fig. 22, the distribution of vorticity

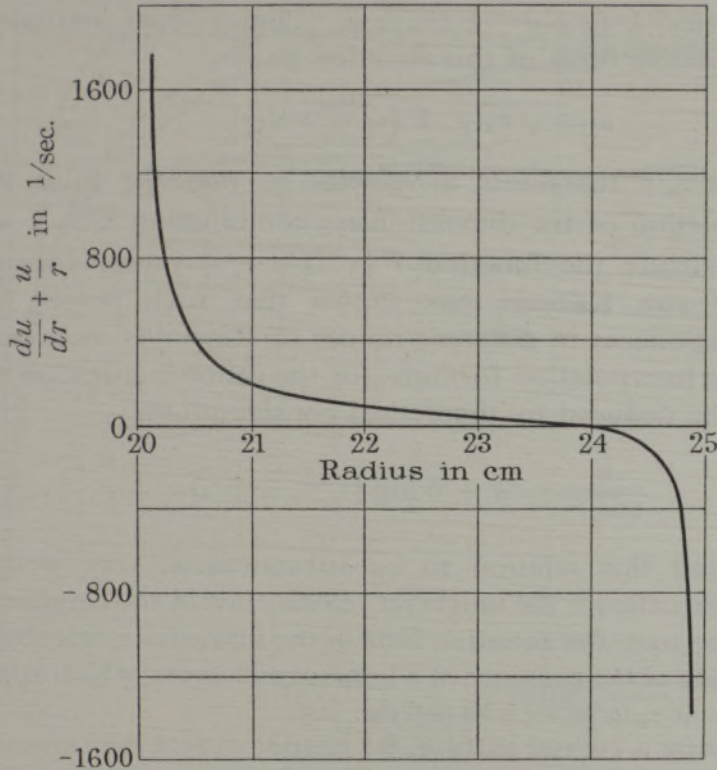


FIG. 22—Vorticity distribution in channel II

over the cross-section is represented. First we notice that the slope of the vorticity has the same sign through the cross-section. We remember in Prandtl's theory the difficulty that the shearing stress and the transfer of moment of momentum, which are supposed to be identical, pass through zero at very different points of the cross-section. Such a discrepancy is avoided in Taylor's theory, since, as we have noted, the rate of change of vorticity has only one sign across the channel. It seems, therefore, that the consideration of the transport of vorticity governed

† 'Proc. Roy. Soc.,' A, vol. 135, p. 678 (1932).

by the pressure drop may give a more adequate starting point for the understanding of the velocity distribution in a curved turbulent flow than the consideration of the transport of momentum and the shearing stress.

17—*Velocity Distributions in the Neighbourhood of the Walls*—It is known that the velocity in the neighbourhood of a smooth straight surface can be expressed as a function of the shearing stress  $\tau_0$  acting on the wall, the distance  $y$  and the two physical parameters, the density  $\rho$  and kinematic viscosity  $\nu$ , *i.e.*,  $u = F(\tau_0 y \rho \nu)$ . Dimensional analysis shows that the only possible form of this function is

$$u = \sqrt{\tau_0/\rho} \cdot F[\sqrt{\tau_0/\rho} y/\nu].$$

The quantity  $\sqrt{\tau_0/\rho}$  represents a velocity so that the ratio  $u/\sqrt{\tau_0/\rho}$  appears as a function of the dimensionless combination  $\sqrt{\tau_0/\rho} y/\nu$ . In order to approximate the function  $F[\sqrt{\tau_0/\rho} y/\nu]$  power formulæ are frequently used von Kármán has shown that such power formulæ with different exponents in different ranges of Reynolds' number are to be considered as interpolation formulæ for the following unique logarithmic law which he deduced by theoretical considerations

$$\frac{u}{\sqrt{\tau_0/\rho}} = a + b \log [\sqrt{\tau_0/\rho} y/\nu].$$

Nikuradse† found this relation to be substantiated very well by his experiments. He called it the universal velocity law in the neighbourhood of a wall. To be sure, the equation fails in the immediate neighbourhood of the wall because of the presence of a laminar sub-layer, which apparently is important for  $\sqrt{\tau_0/\rho} y/\nu < 30$  (*cf.* fig. 20).

In the flow along a curved surface, we cannot expect the ratio  $u/\sqrt{\tau_0/\rho}$  to be a function only of the above-mentioned dimensionless quantities, because with the curvature a new parameter with the dimension of a length enters. We can expect, indeed, that the deviation from the universal distribution is opposite for concave and convex curvatures. In fig. 23 the ratio  $u/\sqrt{\tau_0/\rho}$  is represented as function of  $\sqrt{\tau_0/\rho} y/\nu$  for channel II and the inner and outer cylinders. Unfortunately the exact value of  $\tau_0$  has only been measured for channel II. However, the difference in  $\tau$  are comparatively small so it seemed to be allowable to take a value of  $\tau$  for channel I gained by interpolation between the straight

† 'Proceedings of the 3rd International Congress for Applied Mechanics, Stockholm (1930).

channel and curved channel II. The curves *f* and *g* are obtained in this way and represent the dimensionless velocity distribution in channel I. It is seen that the deviation from the straight flow curve is, in fact, in opposite directions for opposite signs of curvature, and that the magnitude of the deviation increases with curvature.

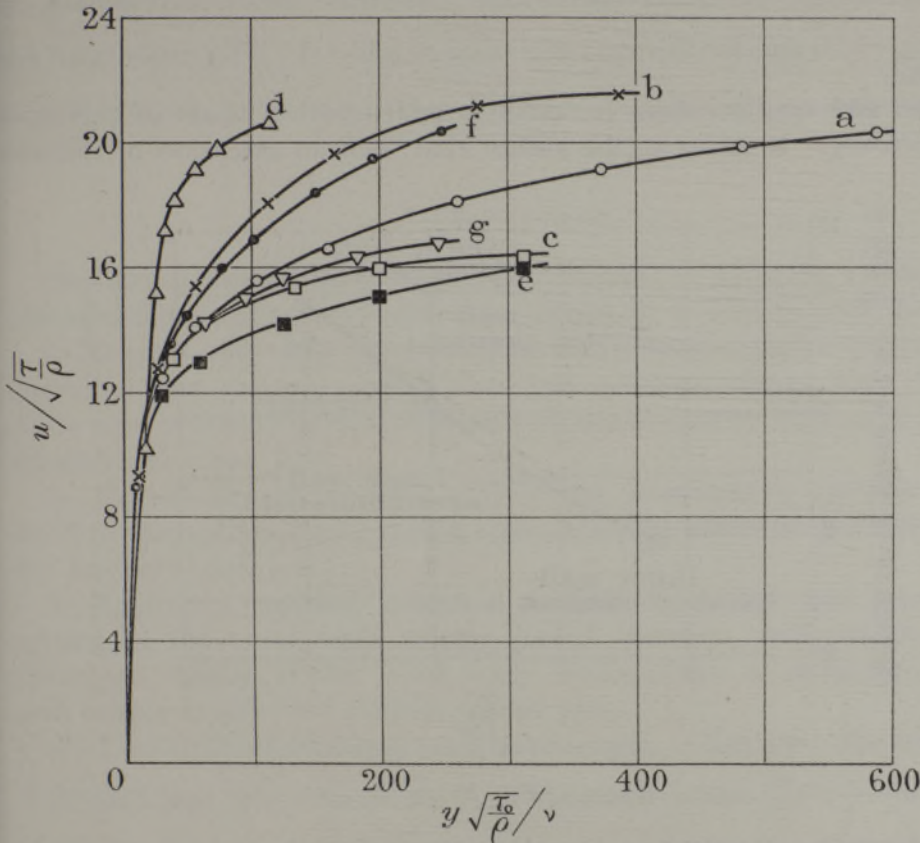


FIG. 23—Dimensionless velocity distribution near wall for curved channel II and concentric cylinder. *a*,  $\circ$  straight; *b*,  $\times$  curved channel II inner; *c*, curved channel II outer; *d*,  $\Delta$  inner rotating cylinder; *e*,  $\blacksquare$  outer stationary cylinder; *f*,  $\bullet$  curved channel I inner; *g*,  $\nabla$  curved channel I outer

As has been mentioned above, the velocity distribution for the straight smooth wall can be approximated in a certain range of Reynolds' numbers by a power law  $\frac{u}{\sqrt{\tau_0/\rho}} = \text{constant} [\sqrt{\tau_0/\rho} y/\nu]^{1/n}$ . It seemed interesting to try such a representation also for flow along the curved surfaces.

In order to express the influence of the curvature, a new dimensionless parameter composed of curvature, shearing stress, and the physical

parameters must be introduced. It is easy to see that the only such dimensionless combination is given by  $\frac{\nu}{r_c \sqrt{\tau_0/\rho}}$  where  $r_c$  denotes the radius of curvature. Fig. 24 represents the smooth curve obtained by plotting the exponent  $n$  of the above power formula against the dimensionless curvature parameter. Straight flow corresponds to  $\frac{\nu}{r_c \sqrt{\tau_0/\rho}} = 0$  and for this case the value of  $n$  is 7.2. The exponent  $n$  has greater and smaller values for positive and negative values of curvature respectively. It seems to the author that such an extension of the uni-

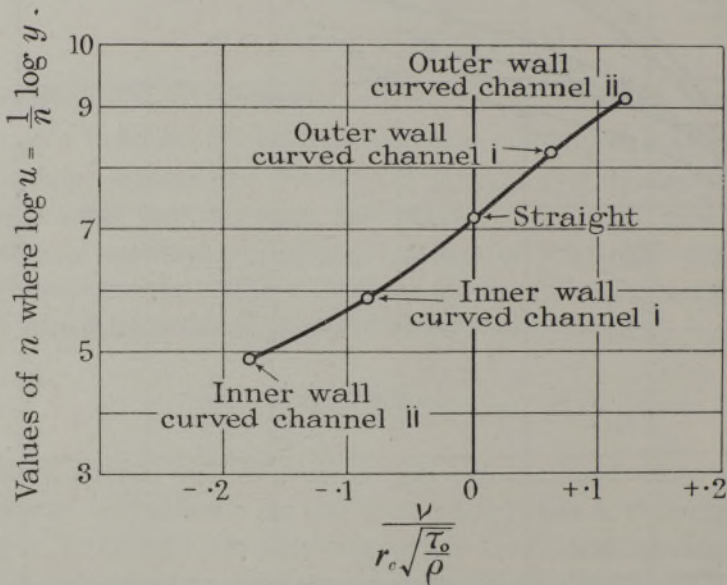


FIG. 24

versal velocity distribution near the wall to the case of curved surfaces has some importance especially for the calculation of boundary layers along such surfaces. Unfortunately the curve plotted does not represent a generally valid universal function since the results obtained for the rotating cylinders do not fit on it.

In fig. 23 the curve  $e$  represents the velocity distribution corresponding to the neighbourhood of the stationary outer cylinder and curve  $d$  the velocity in the neighbourhood of the rotating inner cylinder. It is seen that these curves do not fit in the family of curves obtained for the curved channel. For instance, the curvature in cases  $b$  and  $c$  is almost exactly the same as for cases  $d$  and  $e$  and the curves are distinctly different. It should be noted that the case of the rotating inner cylinder

differs from the case of the flow along a stationary wall since the action of the centrifugal force is quite different in the two cases. However, if a kind of general velocity distribution exists depending only on shearing stress, curvature, and on the physical constants, the curves for the outer concave cylinder and the outer wall of the curved channel II should be practically coincident. It appears that further experiments are necessary to clear up this point. The difference may perhaps be explained by the fact that, in the case of the rotating cylinder, the pressure is constant along the wall, while in the case of the curved channel a pressure drop exists.

### V CONCLUSION

The measurements with these two channels of different curvatures, and with the concentric cylinders have shown the following general facts:

1—There is only slight increase in channel resistance due to the present curvature and there are indications that previous results with curved pipes were probably influenced greatly by the secondary vortices of three-dimensional mean flow.

2—The velocity distributions are strongly influenced by curvature and the flow through the centre region approaches the potential flow following the law  $ur = \text{constant}$ .

3—Rayleigh's stability criterion predicts instability and increased mixing at the outer walls of the curved channels, and stability and decreased mixing at the inner wall. Calculations of exchange factor and mixing length lend support to this idea.

4—Two kinds of similarity may be obtained. Case (a): The channel is divided into two unequal parts, at the point where  $\frac{du}{dr} + \frac{u}{r} = 0$ , at a radius denoted  $r_p$ , and the distance from this point to the channel walls denoted as the effective breadth,  $b_e$ . Similarity between the flow in the two regions of the channels may be obtained by taking the difference between the actual velocity and the potential velocity corresponding to  $ur = (ur)_{\text{max}}$ , dividing by the quantity  $\sqrt{1/\rho \frac{dp}{r_p d\theta} b_e}$ , and plotting against the dimensionless distance from the wall  $y/b_e$ . That both channels appear similar is probably due to the fact that the difference in curvature between the two channels is not great enough to be noticeable for this type of representation. The rotating cylinders cannot be represented in this manner, since the pressure is constant along the walls. Case (b): by means of a difference representation, however, similarity

between the outer wall of the curved channel II and the outer cylinder and between the inner wall of the channel and the inner cylinder has been obtained. The representation differs from that just mentioned in that  $u_p - u$  is divided by  $\sqrt{\tau_0/\rho}$ , where  $\tau_0 =$  measured wall friction. The inner and outer walls are now different and both differ from the corresponding curve for straight flow.

---

## The Vertical Distribution of Atmospheric Ozone in High Latitudes

By A. R. MEETHAM, D.Phil., and G. M. B. DOBSON, D.Sc., F.R.S.

(Received October 15, 1934)

In conjunction with Dr. Götz we have recently given an account\* of a new method of finding the vertical distribution of ozone in the atmosphere, and have used this method to determine the distribution above Arosa, Switzerland. It was found that the average height of the ozone in the atmosphere was much lower than had previously been thought, and these results have since been confirmed by Professor Regener† who has obtained ultra-violet spectra from small balloons up to a height of 30 km. So far the vertical distribution of ozone has not been found anywhere except in Switzerland and in view of the connection between the variations in amount of ozone and atmospheric pressure distribution, and with polar and equatorial air currents, it was of interest to know the distribution in high and low latitudes also. By the kindness of Professor Vegard and the Norwegian Committee for Geophysics arrangements were made to take one of the special photoelectric spectrophotometers‡ for measuring ozone to Tromsø (latitude 69° 40' N., 18° 57' E.) where observations were carried out at the Nordlysobservatorium during May and June, 1934. It had been hoped that by taking observations in the early summer some days with very high ozone content would have been found; unfortunately this did not occur and the ozone content only ranged from 0.230 cm to 0.294 cm, 13 good days' observations being obtained in all.

\* 'Proc. Roy. Soc.,' A, vol. 145, p. 416 (1934).

† 'Phys. Z.,' vol. 35, p. 19 (1934).

‡ Dobson, 'Proc. Phys. Soc. Lond.,' vol. 43, p. 324 (1931).